Received: 16 June 2022 | Revised: 22 December 2022 | Accepted: 5 January 2023

DOI: 10.1111/gbi.12545

gebiology WILEY

ORIGINAL ARTICLE

Protracted oxygenation across the Cambrian–Ordovician transition: A key initiator of the Great Ordovician Biodiversification Event?

Nevin P. Kozik[1] | Seth A. Young[1] | Anders Lindskog[1,2] | Per Ahlberg[2] | Jeremy D. Owens[1]

[1]Department of Earth, Ocean, and Atmospheric Science and National High Magnetic Field Laboratory, Florida State University, Florida, Tallahassee, USA

[2]Department of Geology, Lund University, Lund, Sweden

Correspondence
Nevin P. Kozik, Department of Earth, Ocean, and Atmospheric Science and National High Magnetic Field Laboratory, Florida State University, Tallahassee, Florida 32306, USA.
Email: nkozik@fsu.edu

Funding information
American Chemical Society Petroleum Research Fund; Biirgit and Hellmuth Hertz Foundation; Gyllenstiernska Krapperupsstiftelsen; National Science Foundation; Sloan Research Foundation; Winchester Fund

Abstract

Fluctuations in marine oxygen concentrations have been invoked as a primary driver for changes in biodiversity throughout Earth history. Expansions in reducing marine conditions are commonly invoked as key causal mechanisms for mass extinctions, while increases in marine oxygenation are becoming an increasingly common causal mechanism invoked for biodiversification events. Here we utilize a multiproxy approach to constrain local and global marine paleoredox conditions throughout the late Cambrian–Early Ordovician from two drill core successions in Baltoscandia. Local paleoredox proxies such as manganese concentrations and iron speciation reveal that both sites in the Baltic paleobasin had persistently anoxic and predominantly euxinic (anoxic and sulfidic) bottom water conditions throughout the study interval. Corresponding trace metal datasets indicate nuanced contraction and expansion of global anoxic and euxinic conditions along continental margins during the late Cambrian–Early Ordovician. Lastly, thallium isotope data from these locally reducing sections suggest a global expansion of oxygenated shelf and deeper marine environments from the late Cambrian into the Early Ordovician. This evidence for increasingly oxic marine environments coincides with increases in burrowing depth and tiering in marine animals, as well as diversification of body fossils throughout this ~8-million-year interval. The collective geochemical datasets provide some of the first direct paleoredox evidence for an increase in marine oxygen concentrations as a key mechanism for the Ordovician radiation of marine life.

KEYWORDS
anoxia, biodiversity, Cambrian, molybdenum, Ordovician, thallium isotopes, vanadium

1 | INTRODUCTION

Over the last several decades, increased attention surrounding the Ordovician has identified the largest increase in marine biodiversity in the Phanerozoic, named the Great Ordovician Biodiversification Event (GOBE) or Ordovician Radiation. Several studies have identified major species and genus radiations. However, the timing and nomenclature surrounding different aspects of the trends in diversity are still widely debated, as is also the case with primary causal mechanisms (Rasmussen et al., 2019; Servais et al., 2021; Stigall et al., 2019). The GOBE was an impressive near quadrupling of genus-level diversity of marine animals alongside an increase in the utilization of new niches and ecologic space, entailing deeper burrowing and taller suspension feeding (i.e., greater tiering) (Bottjer &

Ausich, 1986; Droser & Bottjer, 1993). Detailed studies focused on the biodiversification of various marine clades reveal that planktonic life modes diversified earlier on during the GOBE, as compared to nektonic or benthic life modes which primarily diversified later in the Ordovician (Deng et al., 2021; Servais et al., 2010). This increase in diversity at the base of the food chain has been postulated to have fueled the diversification of higher trophic level organisms in later pulses of the GOBE (Achab & Paris, 2007; Saltzman et al., 2011; Servais et al., 2008). Other causal mechanisms behind the changes in biodiversity are also a subject of debate, with suggestions including several environmental factors and influences ranging from global climatic cooling, changes in nutrient cycling, higher eustatic sea level, meteorite impacts, and enhanced levels of marine oxygen (Edwards et al., 2017; Schmitz et al., 2008; Servais et al., 2010; Stigall et al., 2019; Trotter et al., 2008). The rapid increase in biodiversification during the GOBE followed numerous globally recognized extinctions of Cambrian biomere faunas, which are often associated with positive carbon isotope excursions (CIEs), with the most well studied of these CIEs being the Steptoean Positive Carbon Isotope Excursion or SPICE (Pulsipher et al., 2021; Saltzman et al., 2015). These extinctions continued into the Early Ordovician with the last biomere events occurring in the latest Tremadocian (~477 Ma).

Here we will utilize recent nomenclature for these changes in biodiversity, with the initiation phase of the GOBE (also referred to as the pre-GOBE phase) occurring just after the Cambrian–Ordovician boundary, within the early Tremadocian through late Floian (~486–471 Ma; Stigall et al., 2019; Deng et al., 2021). The peak diversity or main phase of the GOBE occurred later in the Dapingian to Darriwilian (~471–458 Ma; Rasmussen et al., 2019; Stigall et al., 2019; Deng et al., 2021). Paired carbon and sulfur isotopes, I/Ca ratios, and sea-level reconstructions indicate that at least two of the biomere extinction events coincided with transgression events, which, in turn, expanded anoxic and euxinic (anoxic + sulfidic) deeper-sourced waters into shallower shelf environments (Edwards et al., 2018; Gill et al., 2011; Palmer, 1984; Saltzman et al., 2015). Currently, paleoredox conditions in the latest Cambrian–Early Ordovician (Stage 10–early Tremadocian; ~491–482 Ma) are poorly constrained. In this study, we present new iron speciation, trace metal concentrations (manganese, vanadium, and molybdenum), and thallium isotope datasets ($\varepsilon^{205}Tl_{auth}$) from organic-rich shale sequences spanning the late Furongian through mid-Tremadocian stages in Baltoscandia. The two drill-core successions from southern Sweden, the Grönhögen-2015 and Tosterup-2, have been the subject of previous biostratigraphic and carbon isotopic studies. Both drill cores have good records of geographically widespread or globally utilized trilobite and graptolite faunas, as well as the globally recognized SPICE and TOCE/HERB CIEs (Ahlberg et al., 2019; Terfelt et al., 2014; Zhao et al., 2022). Our integrated, multiproxy geochemical dataset is one of the first to constrain local and global marine redox conditions throughout the late Cambrian—Early Ordovician transition, allowing for refined interpretations of the role that marine oxygen may have played in the initiation of GOBE.

2 | BACKGROUND

Our study sites originate from the western margin of the Baltic paleocontinent, which was located at mid to high (~50°) southern paleolatitudes throughout the late Cambrian and Early Ordovician (Torsvik et al., 2012). The Baltic Basin is thought to have been directly connected to the Iapetus Ocean to the paleo-western direction (Figure 1). Both drill cores are from southern Sweden, and were retrieved ~180 km from one another, with the Grönhögen-2015 drill core originating from the Island of Öland and the Tosterup-2 drill core from southeastern Skåne (Figure 1; Terfelt et al., 2014; Ahlberg et al., 2019). Our study focuses chiefly on the Alum Shale Formation within each drill core, which unconformably overlies the "lower" Cambrian (unnamed Series 2, Stage 4) Gislöv Formation in Skåne and the "middle" Cambrian (Miaolingian Series, Wuliuan Stage) Borgholm Formation on Öland. The sequences were deposited during relatively stable tectonic conditions (Nielsen & Schovsbo, 2011). The Alum Shale Formation in both cores consists primarily of finely laminated, organic-rich black shales, with subordinate limestone beds and minor limestone concretions (commonly referred to as "orsten"

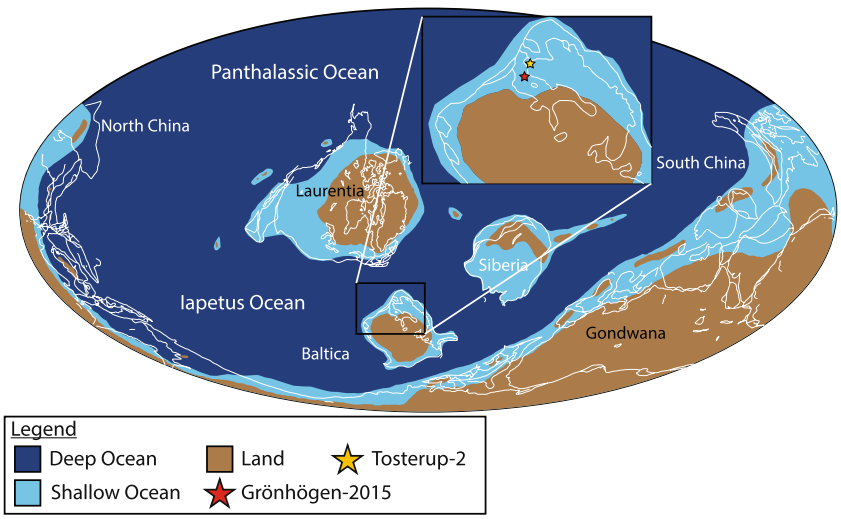

FIGURE 1 Paleogeographic reconstruction of the late Cambrian with approximate location of study sites marked in red and yellow stars. Modified from Scotese (2001)

or stinkstone), and has been interpreted to be deposited in an extensive, level-bottomed and moderately deep epeiric sea that covered most of Scandinavia and surrounding areas, that is, all of (present-day) western Baltica (Cocks & Torsvik, 2005; Nielsen et al., 2020; Zhao et al., 2022).

Between the two cores, the Alum Shale Formation spans a mostly complete record that extends from the Guzhangian into the lowermost Tremadocian Stage (upper Cambrian–Lower Ordovician). The studied and sampled interval of the Grönhögen-2015 core extends down into the upper Cambrian *Olenus truncatus* trilobite Biozone of the Paibian Stage but the Furongian succession is incomplete and there are several substantial gaps of variable magnitudes, with the most notable unconformity at the Cambrian–Ordovician boundary (Ahlberg et al., 2019). More specifically, previous biostratigraphic studies have identified unconformities between the *Olenus truncatus* and *Parabolina brevispina* biozones, the *Parabolina spinulosa* and *Sphaerophthalmus? flagellifer* biozones, and the *Ctenopyge tumida* and *C. linnarssoni* biozones, indicating several gaps within the Jiangshanian Stage and Stage 10 (Ahlberg et al., 2019; Zhao et al., 2022). In addition, detailed biostratigraphic study of the Grönhögen-2015 core has revealed that approximately the upper half of Stage 10 through lowermost portion of the Tremadocian are missing at the associated unconformity (the *Peltura paradoxa*/*Parabolina heres megalops* through *Acerocare ecorne* trilobite biozones are not recorded). Due to these unconformities within the Grönhögen-2015 core, the uppermost portion of the TOCE/HERB negative CIE is truncated (incomplete) and excludes the return to baseline values in the uppermost Stage 10. The lowermost portion of the Tosterup-2 core biostratigraphically overlaps with the Grönhögen-2015 core via the *Ctenopyge linnarssoni* trilobite Biozone and furthermore contains a virtually complete stratigraphic succession across the Cambrian–Ordovician boundary, as constrained by latest Cambrian trilobites and Early Ordovician graptolites (Terfelt et al., 2014).

2.1 | Iron geochemistry

Iron geochemistry from organic-rich shales is a common tool in constraining local redox conditions utilizing the ratios of various Fe phases. Reducing marine settings generally contain higher amounts of "highly reactive" iron, in the phases of pyrite, siderite, and other Fe-(oxyhydr)oxides (i.e., ferrihydrite, lepidocrocite, goethite, hematite, and magnetite). Thus, the ratio between highly reactive iron (Fe_{HR}) to total iron (Fe_T) can indicate local anoxia within the depositional basin (Poulton & Canfield, 2005; Raiswell et al., 2018). Ratios of Fe_{HR}/Fe_T higher than 0.38 have been shown to occur under anoxic conditions; however, values between 0.22 and 0.38 may have complications, because high sedimentation rates can mask the enrichment of highly reactive iron. In addition, late diagenetic alteration may also transfer highly reactive iron into poorly reactive, chiefly silicate-bound iron (Pasquier et al., 2022; Raiswell et al., 2018). Once sediments are determined to be deposited under anoxic conditions, ratios between pyrite iron (Fe_{pyr}) and Fe_{HR} are used to determine whether the anoxic conditions were ferruginous (anoxic and Fe^{2+} rich, or sulfate limited) or euxinic (anoxic and sulfide rich, or iron limited); values of Fe_{pyr}/Fe_{HR} above 0.70 are likely to have been deposited under euxinic conditions, whereas values below this were deposited in ferruginous conditions.

2.2 | Trace metal geochemistry

Sedimentary trace metal concentrations have been used to infer changes in both local and global redox conditions, nutrient availability, and/or productivity (Algeo & Lyons, 2006; Anbar et al., 2007; Reinhard et al., 2013; Scott & Lyons, 2012; Tribovillard et al., 2006). When paired, iron geochemistry and trace metal concentrations form a powerful tool to interpret global paleoredox changes as iron speciation provides an independent constraint on local redox conditions which may influence the enrichments of trace metals. In this study, we focus primarily on the elemental cycles of manganese (Mn), vanadium (V), and molybdenum (Mo), each of which have differing reduction potentials, and thus have slightly different responses to changes in local and global redox conditions.

The rapid response to local reducing conditions allows Mn to be used as a local redox proxy. Under slightly reducing conditions, solid Mn-oxide ($Mn^{3+/4+}$) is quickly reduced to aqueous Mn^{2+} due to its high redox potential (Algeo & Maynard, 2008; Froelich et al., 1979; Rue et al., 1997). Due to the rapid oxidation, Mn has a shorter residence time (~0.06 kyr) than ocean mixing (~1–2 kyr), thus limiting its use as a global paleoredox proxy (Tribovillard et al., 2006). Mn-oxides, upon being reductively dissolved in either the water column or within marine sediments, liberate aqueous Mn^{2+} that can be either diffusively recycled into the water column above and/or be precipitated into Mn-bearing minerals such as sulfides and/or carbonates (Algeo & Maynard, 2008; Calvert & Pedersen, 1996; Force & Maynard, 1991). Concentrations less than the average oxic shale value of ~850 ppm (parts per million) of Mn generally indicate sediments deposited under reducing conditions, while values above this threshold are generally associated with oxidizing conditions (Force & Maynard, 1991; Turgeon & Brumsack, 2006). In addition, we use thallium (Tl) isotopic compositions to infer changes in global Mn-oxide burial, which can be related back to changes in global bottom-water oxygen conditions (see Section 2.3).

Unlike manganese, V has a longer residence time of ~50 to 100 kyr. Within oxic waters, vanadium forms stable HVO_4^{2-} and $H_2VO_4^-$ ions (with V^{5+} oxidation state) that behave mostly conservatively, but can adsorb to Mn and Fe-oxides (Tribovillard et al., 2006). However, under mildly reducing conditions, V^{5+} is reduced to V^{4+} which forms insoluble $VO(OH)_2$ and $VO(OH)_3^-$ which can react with humic acids to form solid precipitates, both of which and can be buried within sediments. Under euxinic conditions, V^{4+} can be further reduced to V^{3+} and be precipitated into solid V_2O_3 or V-oxyhydroxides (Tribovillard et al., 2006). Due to the initial reduction of V under low oxygen conditions, enrichment is not dependent on the presence of sulfide and thus has

been used to indicate changes in global anoxia when paired with another proxy that can fingerprint changes in sulfidic conditions (Owens et al., 2016; Young et al., 2020).

Molybdenum has a relatively long residence time of ~450 kyr and is the most abundant transition metal in the modern oceans (Tribovillard et al., 2006). Similar to vanadium, Mo forms stable molybdate (MoO_4^{2-}) ions under oxic conditions that can adsorb onto Mn and Fe-oxides (Algeo & Tribovillard, 2009). Under oxic conditions, sedimentary Mo concentrations are similar to crustal values of ~2 ppm (Taylor & McLennan, 1995). In the presence of H_2S, Mo is efficiently enriched within sediments through the reduction in molybdate into thiomolybdates (MoO_xS_{4-x}, where x = 0 to 3) which are particle reactive, and prone to scavenging by sulfides and sulfur-rich organic molecules (Erickson & Helz, 2000). Mild enrichments, which entail concentrations below 25 ppm, are generally thought to reflect sulfide restricted to sediment porewaters, while moderate enrichments entail concentrations between 25 and 100 ppm that reflect potentially euxinic conditions with some complications (Scott & Lyons, 2012). These complications include deposition under either intermittently euxinic/sulfidic conditions, enrichments that were diluted via high sedimentation rates, had variability in water column pH, or most importantly may have experienced changes in dissolved concentrations within the water column or global marine inventory (Hardisty et al., 2018; Scott & Lyons, 2012). Lastly, highly enriched sediments, that is, sedimentary concentrations of Mo greater than 100 ppm, are considered a strong indicator of water column euxinia with little to no complications discussed previous, that is, nonrestricted connection to open marine conditions and strongly euxinic redox chemistry (Hardisty et al., 2018; Scott & Lyons, 2012).

The use of enrichment factors is a common tool to compare the authigenic enrichment of redox sensitive trace metals with varying upper continental crustal concentrations, by normalizing a given element to aluminum (a conservative and typically non-reactive element). Here we employ the use of enrichment factors, following the convention of Algeo and Tribovillard (2009): $X_{EF} = [(X/Al)_{sample}/(X/Al)_{PAAS}]$, where X is the concentration of a given redox sensitive metal and Al is the concentration of aluminum. Sample concentrations are then normalized to the composition of post-Archean average shale, or PAAS (Taylor & McLennan, 1995). Enrichment factors ≈1 are considered to represent no enrichment, but rather values equal to background sedimentation, while enrichment factor values ≥3 are generally considered to be noticeable, and lastly, enrichments ≥10 are considered substantial (Algeo & Tribovillard, 2009).

2.3 | Thallium isotopes

Sedimentary Tl isotopic compositions are an emergent paleoredox proxy that have been utilized in several studies to identify changes in global seafloor Mn-oxide burial through Earth history (Bowman et al., 2019; Fan et al., 2020; Newby et al., 2021; Ostrander et al., 2017, 2019, 2020; Them et al., 2018). Tl isotopic compositions, reported as $\varepsilon^{205}Tl_{auth} = ({}^{205/203}Tl_{sample} - {}^{205/203}Tl_{NIST\text{-}997})/{}^{205/203}Tl_{NIST\text{-}997} \times 10^4$, of modern seawater are homogeneous ($\varepsilon^{205}Tl_{seawater} = -6 \pm 0.3$) due to a longer residence time of ~18.5 kyr compared to ocean mixing of ~1–2 kyr, as well as presenting a conservative seawater profile (Owens, 2020; Owens et al., 2017). Bulk crustal values for Tl have been documented to be $\varepsilon^{205}Tl_{bulk} = -2 \pm 1.0$ (Nielsen et al., 2005). The modern Tl isotopic mass balance suggests that changes in seawater isotopic compositions are primarily controlled by the output fluxes and associated fractionations; the first being the alteration of oceanic crust (AOC) ($\varepsilon^{205}Tl_{AOC} = -12$ to -6) and the second being the burial of Mn-oxides, particularly the Mn-oxide, birnessite, ($\varepsilon^{205}Tl_{Mn\text{-}oxides} = +6$ to $+12$), while the third and final output is anoxic, but non-sulfidic sediments. Theminor output flux of anoxic sediments is not thought to produce a major fractionation, but rather potentially record seawater Tl isotopic compositions (Fan et al., 2020; Owens et al., 2017; Wang et al., 2022). Meanwhile, most inputs of Tl are isotopically similar to bulk crustal material and thus are not thought to be major controlling factors for the Tl isotopic budget ($\varepsilon^{205}Tl_{inputs} = \sim -2$; Owens et al., 2017; Owens, 2020). Importantly, changes in the burial flux of Mn-oxides have the largest isotopic difference between seawater and output flux ($\Delta_{seawater\text{–}Mn\text{-}oxides} = 16$), as well as occurring on geologically short (less than multi–million–year process) timescales, when compared to the difference between changes in AOC output fluxes and seawater ($\Delta_{seawater\text{–}AOC} = -1.2$) that occurs on tectonic timescales. Originally, sediments deposited in open marine settings under permanently euxinic settings have been shown to capture the overlying seawater values (within analytical error; Owens et al., 2017), which is likely related to the adsorption of Tl to authigenic pyrite precipitation (Fan et al., 2020; Nielsen et al., 2011). A recent study has also shown that anoxic, but non-sulfidic sediments may also capture contemporaneous seawater Tl isotopic values, so long as sediments are sufficiently reducing to reductively dissolve all non-oxide forms of Mn and generally contain Mn_{EF} values ≤5 (Wang et al., 2022).

3 | MATERIALS AND METHODS

3.1 | Sample collection and preparation

The Grönhögen-2015 core is housed at the Swedish Geological Survey (SGU) and the Tosterup-2 core is housed at the Department of Geology, Lund University, Sweden, where samples and detailed lithologic descriptions were undertaken for this study. Fine-grained shale samples were taken at ~25 cm intervals for geochemical analyses to be conducted at Florida State University (FSU) and the National High Magnetic Field Laboratory (NHMFL). The samples were selected from horizons without obvious (late-)diagenetic alteration, such as secondary recrystallization, calcite veins and pyrite nodules. Samples were cleaned in an ultrasonic bath of deionized water (18.2 MΩ) to remove weathered surface or drilling mud residue, then dried and powdered using an agate mortar and pestle.

3.2 | Organic carbon isotopes

A total of 78 samples were analyzed for $\delta^{13}C_{org}$ from the Grönhögen-2015 (n = 29) and Tosterup-2 (n = 49) cores. Approximately 0.5 g of powdered sample was weighed into clean centrifuge tubes and reacted with 6 N HCl to remove any carbonate minerals. Samples were acidified and washed with deionized water (18.2 MΩ) three times and left to dry in a 70°C oven overnight. Residues were then homogenized and weighed into tin cups for isotopic analysis. Organic carbon isotopic analysis was measured using a Carlo Erba Elemental Analyzer coupled to a ThermoFinnegan Delta Plus XP isotope ratio mass spectrometer (IRMS) via a Conflo-III device at NHMFL-FSU. Sample precision and calibration of data was assessed during routine analysis of laboratory standards that are calibrated against IAEA standards and are reported in standard delta-notation (δ) with units reported in per mill (‰) relative to VPDB (Vienna Pee Dee Belemnite). Organic carbon isotope standards at NHMFL-FSU include Acetanilide (−29.2‰), Urea-2 (−8.3‰), and WYSTD (−12.7‰). Analytical precision for $\delta^{13}C_{org}$ is ±0.2‰ and ±0.7% for %C (1σ) or better. Weight percent of total organic carbon in samples is determined by comparison to voltages for the CO_2^+ ion beam intensities for masses 44, 45, and 46 between unknown and known wt% of carbon of the gravimetric standard acetanilide analyzed during the same sequence. The uncertainty of these TOC measurements is better than ±5%.

3.3 | Pyrite sulfur extraction

Sedimentary pyrite was extracted from 78 samples (the same selected for carbon analysis) following a modified chromium reducible sulfur extraction procedure from Brüchert and Pratt (1996). Powdered samples (~0.5–2.0 g) were weighed into glass extraction flasks, where powders were reacted with a mixture of 70 mL of 12 M HCl and 30 ml of 1.0 M of $CrCl_2$ that was continuously heated and agitated for 2–3 h. Any evolved H_2S gas was passed through a mixture of 0.1 M sodium citrate buffered to a pH of 4, then passed through a 0.1 M $AgNO_3$ solution to precipitate Ag_2S. The $AgNO_3$ and Ag_2S were filtered, rinsed (with 18.2 MΩ deionized water), dried, and weighed for concentration determinations. Total amounts of Ag_2S precipitate were gravimetrically determined to calculate wt% pyrite using the quantitative conversion and stoichiometry of Fe_2S into Ag_2S, and subsequently used to calculate pyrite Fe (Fe_{pyr}, see more in Section 3.4).

3.4 | Iron speciation

A total of 78 samples (the same as above) were analyzed for sequential Fe extractions (Fe speciation), following the procedures outlined by Poulton and Canfield (2005). Powdered samples were weighed (~0.1 g) into 15 ml centrifuge tubes. The first extraction used 10 ml of 1.0 M sodium acetate, buffered to pH 4.5 was allowed to react with samples for 48 h to extract Fe from carbonate minerals (Fe_{carb}). Second, 10 ml of 0.29 M sodium dithionite buffered to pH 4.8 with 0.35 acetic acid and sodium citrate was reacted with samples for 2 h to extract Fe from oxides and oxyhydroxides (Fe_{ox}). Lastly, residues were reacted with 0.2 M ammonium oxalate and 0.17 M oxalic acid buffered to pH 3.2 with ammonium hydroxide for 6 h to extract Fe from magnetite (Fe_{mag}). Following each step, samples were centrifuged, and supernatant was saved for analysis. Each sample was rinsed with 18.2 MΩ deionized water, centrifuged, and decanted before each extraction. The supernatant from each extraction was diluted with 2% ultrapure HNO_3 and analyzed for Fe concentrations using an Agilent 7500cs inductively coupled plasma mass spectrometer (ICP-MS) at the NHFML-FSU. Highly reactive Fe (Fe_{HR}) was calculated from the sum of all species: $Fe_{carb} + Fe_{ox} + Fe_{mag} + Fe_{pyr}$. Duplicate samples had reproducibility of 7% for the entire extraction method.

3.5 | Trace metal concentrations

Trace metal concentrations were analyzed for the same samples selected for the aforementioned analyses, through multi-acid digestion. Samples were weighed (~100 mg) into Savillex beakers and microwave digested using a CEM MARS 6 microwave system to digest organic carbon. Samples were subsequently dissolved completely using various combinations of trace metal-free HNO_3, HCl, and HF. Acids were allowed to react with samples with heat (~120–180°C) for 24–48 h and dried down between adding different and additional acids. Following complete dissolution of sample powder, samples were dried down and dissolved into 2% HNO_3 and analyzed on an Agilent 7500cs ICP-MS for trace metal concentration at NHFML-FSU. Samples were compared to USGS standards SDO-1, SCO-1, and SGR-1 that were dissolved simultaneously with samples and were all within accepted reported analytical ranges for the analyzed elements. All results are reported as ppm with a precision of ±5% or better for Mn, V, Fe, and Mo.

3.6 | Thallium isotopes

A subset (45 total) of the aforementioned samples was analyzed for thallium isotopes following the modified procedure outlined by Nielsen et al. (2011) and Owens et al. (2017). Briefly, the samples that were chosen for trace metal analysis were weighed (100 mg) into clean Savillex beakers and allowed to react with 2 M HNO_3 at 130°C for 12 h to separate leachable Tl adsorbed to pyrite. The supernatant from the leaching was then purified of Pb using micro-columns filled with Bio-Rad AG1-X8 resin following established column chemistry procedures (Nielsen et al., 2011; Owens et al., 2017). Thus, presented Tl isotopic compositions represent the authigenic fraction, $\varepsilon^{205}Tl_{auth}$. Samples were subsequently analyzed for Tl concentration using an Agilent 7500cs ICP-MS, then spiked with NIST-SRM-981 Pb to track mass bias during mass spectrometry analysis (Nielsen

et al., 2005). Tl isotopes were analyzed with a Neptune multicollector MC-ICP-MS using an Aridus II autosampler at the NHMFL-FSU. All Tl isotopes are reported as ε^{205}Tl, and USGS SCO-1 reference material was analyzed to monitor long-term precision of the entire method which was $\varepsilon^{205}\text{Tl} = -3.00 \pm 0.3$ (2σ; nearly identical to published data by Owens et al. (2017)). All samples reported here have an uncertainty of less than 0.5 (2σ, based on 2 or more replicate analyses); however, conservatively, any samples with uncertainty <0.3 adopted this uncertainty as this is the error for the long-term geostandard value for the entire method.

4 | RESULTS

4.1 | Grönhögen-2015 core

High-resolution organic carbon isotope data for the Grönhögen-2015 core has already been published (Ahlberg et al., 2019), documenting the globally recognized SPICE and TOCE/HERB CIEs, and our new TOC measurements for all samples have an average of ~10.5 ± 1 wt% TOC, which range between 5.5 and 14.4 wt% for the entire core (Figure 2; DR Table S1). The concentrations of Mn throughout the Grönhögen-2015 core are relatively low, with a total core average of 334 ppm (min. 198 ppm, max. 704 ppm). The trends of Mn_{EF} are nearly identical to that of Mn concentrations, with Mn_{EF} generally ≤1, with a total core average of 0.5 (min. 0.41, max. 2.2). Iron speciation (Fe_{HR}/Fe_T) shows relatively high values (≥0.38) within the *O. truncatus* through *C. tumida* biozones and fall to average values of ~0.31 throughout the rest of the analyzed portion. Meanwhile Fe_{pyr}/Fe_{HR} values are all above 0.8, excluding two points within the *C. linnarssoni* and "*Adelograptus*" biozones (Figure 2). Trace metal concentrations show large enrichments of Mo throughout Cambrian strata, with an average of 132 ppm (Figure 2.; min. 84 ppm, max. 227 ppm), and a sudden decrease in overall concentration within Ordovician strata to an average of 86 ppm (min. 38 ppm, max. 199 ppm). Here we document nearly mirrored trends between the enrichment factors of Mo and its concentrations; Mo_{EF} throughout the Cambrian are consistently higher, with an average of 106 (min. 55, max. 164) than that of overlying Ordovician shales, with an average of 58 (min. 22, max. 126). Concentrations of V show inverse macro-scale trends as Mo, with smaller enrichments within Cambrian strata with an average of 929 ppm (Figure 2; min. 340 ppm, max. 1058 ppm) and a sudden increase in V enrichments to an average of 1983 ppm (min. 288 ppm, max. 3585 ppm). Similar to the enrichment factors of molybdenum, trends in V_{EF} show nearly identical macroscopic scale trends to its concentrations, with relatively smaller enrichments within the Cambrian, with an average of 17 (min. 7, max. 54), with overlying Ordovician strata containing higher average enrichments, with an average of 32 (min. 4, max. 54). Lastly, $\varepsilon^{205}\text{Tl}_{auth}$ shows an increasing trend within the *O. truncatus* through *C. tumida* biozones, from values of approximately −2.5 to −0.70, and subsequently show a decreasing trend to values of −2.71 in the lowermost portion of the "*Adelograptus*" Biozone, where it comes to nearly invariant values of an average of −2.72.

4.2 | Tosterup-2 core

Detailed organic carbon isotope data for a portion of the Tosterup-2 core have already been published (Figure 3; Terfelt et al., 2014).

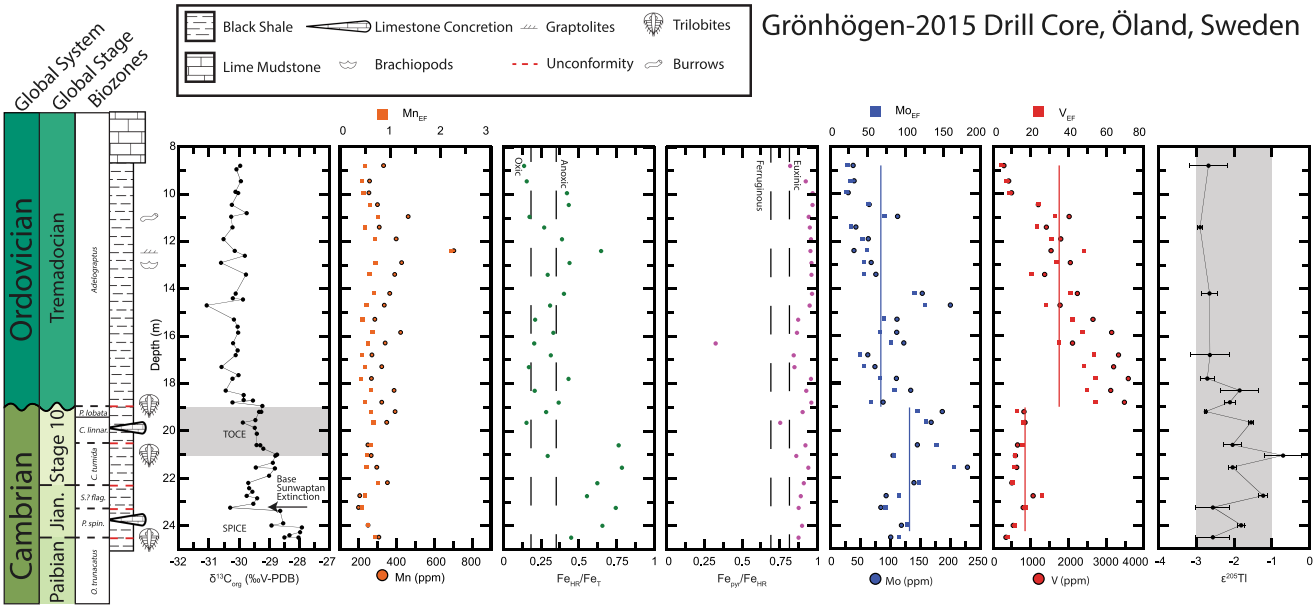

FIGURE 2 Furongian and Tremadocian geochemical profiles of the Grönhögen-2015 drill core. Trilobite (Cambrian) and graptolite (Ordovician) biozones are plotted from previous biostratigraphic studies, separated by unconformities marked as orange dashed lines (Ahlberg et al., 2019). Horizontal gray bar indicates the TOCE negative excursion. Vertical gray bar represents bulk crustal isotopic value of Tl

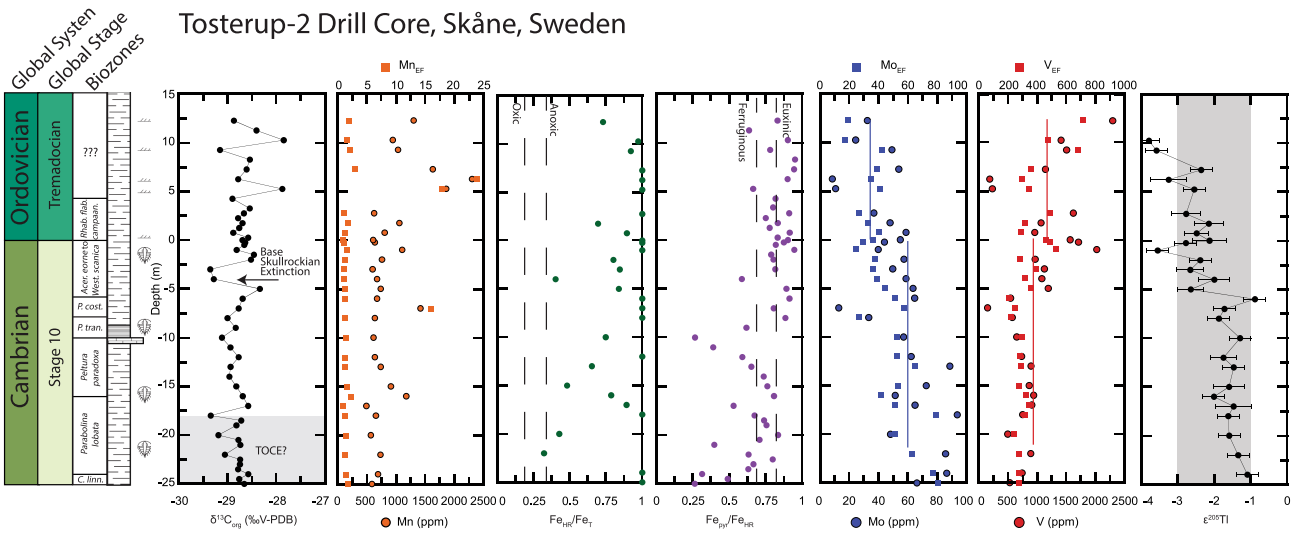

FIGURE 3 Upper Furongian and Tremadocian geochemical profiles of the Tosterup-2 drill core. Trilobite (Cambrian) and graptolite (Ordovician) biozones are plotted from previous biostratigraphic studies (Terfelt et al., 2014). Horizontal gray bar indicates the putative TOCE negative excursion. Vertical gray bar represents bulk crustal isotopic value of Tl

However, our new and expanded $\delta^{13}C_{org}$ profile potentially show the rising limb of the TOCE/HERB CIE within the *C. linnarssoni* to *Parabolina lobata* trilobite biozones, along with TOC measurements showing an average 1.5 ± 0.5 wt% and ranges between 0.5 and 2.5 wt% throughout the drill core (Figure 3; DR Table S2). Within the uppermost *P. lobata* Biozone, $\delta^{13}C_{org}$ reveals relatively invariant values averaging −28.8‰ with a minimum of −29.4‰ and a maximum of −27.9‰. The concentrations of Mn throughout the Tosterup-2 core are higher than that of the Grönhögen-2015 core, with a total core average of 912 ppm (min. 496 ppm, max. 2307 ppm). Similarly, Mn_{EF} is also higher than the Grönhögen-2015 core, with a total core average of 3.3 (min. 0.98, max. 23). For iron speciation, Fe_{HR}/Fe_T shows nearly all values ≥0.38 throughout the core, except for a singular data point of 0.32 within the *P. lobata* Biozone. Meanwhile, Fe_{pyr}/Fe_{HR} shows an increasing trend through the *C. linnarssoni* to *P. lobata* biozones, from a minimum of approximately 0.25, to an average of 0.70, and a maximum of 0.83. A decreasing trend is present within the *Peltura paradoxa* Biozone to a minimum of 0.27, and then an increasing trend is seen within the *Peltura transiens* and *P. costata* biozones (*Acerocarina granulata–Peltura costata* Biozone in the revised zonation of Nielsen et al., 2020) to an average of 0.80 throughout the rest of the core. Trace metal concentrations show moderate enrichments in Mo throughout the Cambrian, with an average of 60 ppm (Figure 3; min. 8 ppm, max. 65 ppm) with a decrease in average of 38 ppm (min. 8, max. 58) within Ordovician strata. Trends of Mo_{EF} show similar trends to its concentrations, with a Cambrian average of 50 (min. 29, max. 90), and a lower average of 32 (min. 17, max. 42) in the overlying Ordovician shales. Concentrations of V show an inverse relationship to that of Mo, with an average of 888 ppm (Figure 3; min. 149 ppm, max. 2024 ppm) within Cambrian strata with a decrease to an average of 1120 ppm (min. 184 ppm, max. 2300 ppm) within Ordovician strata. Trends of V_{EF} show similar trends to its concentrations, with a Cambrian average of 312 (min. 220, max. 553), with higher enrichments in overlying Ordovician strata with an average of 443 (min. 289, max. 716). Lastly, $\varepsilon^{205}Tl_{auth}$ shows a steady decreasing trend to lighter isotopic values in the Lower Ordovician (Tremadocian) from heavy values in the upper Cambrian (upper Jiangshanian Stage). Specifically, average $\varepsilon^{205}Tl_{auth}$ = −1.5 within the *C. linnarssoni* through *Westergaardia scanica* biozones that subsequently decline steadily through the upper *W. scanica* trilobite Biozone and the *Rhabdinopora flabelliformis parabola* graptolite Biozone (*Rhabdinopora campanulatum* Biozone of Maletz et al., 2022). The lowest $\varepsilon^{205}Tl_{auth}$ = ~ −4.0 occurs within the Lower Ordovician black shales of the *Rhabdinopora flabelliformis parabola* Biozone (= *R. campanulatum* Biozone).

5 | DISCUSSION

Assessing the preservation of geochemical signatures is paramount to ensure that subsequent interpretations of the Cambrian–Ordovician boundary interval data reflect true paleoredox landscapes. The use of geochemical cross-plots is a widely used tool to assess the nature of redox proxies. Cross-plots of the Grönhögen-2015 and Tosterup-2 cores show weak to moderate correlations between given geochemical parameters (Figure 4). Linear relationships between $\delta^{13}C_{org}$ and TOC wt % can be useful in determining thermal heating or oxidative loss of organic compounds; however, very weak correlations (R^2 = 0.02 for both cores) between these parameters suggest little thermal alteration (Hayes et al., 1999; Meyers, 1994).

There is a slight negative correlation between Mn concentrations and Tl isotopic compositions (R^2 = 0.19), as well as an elevated Mn

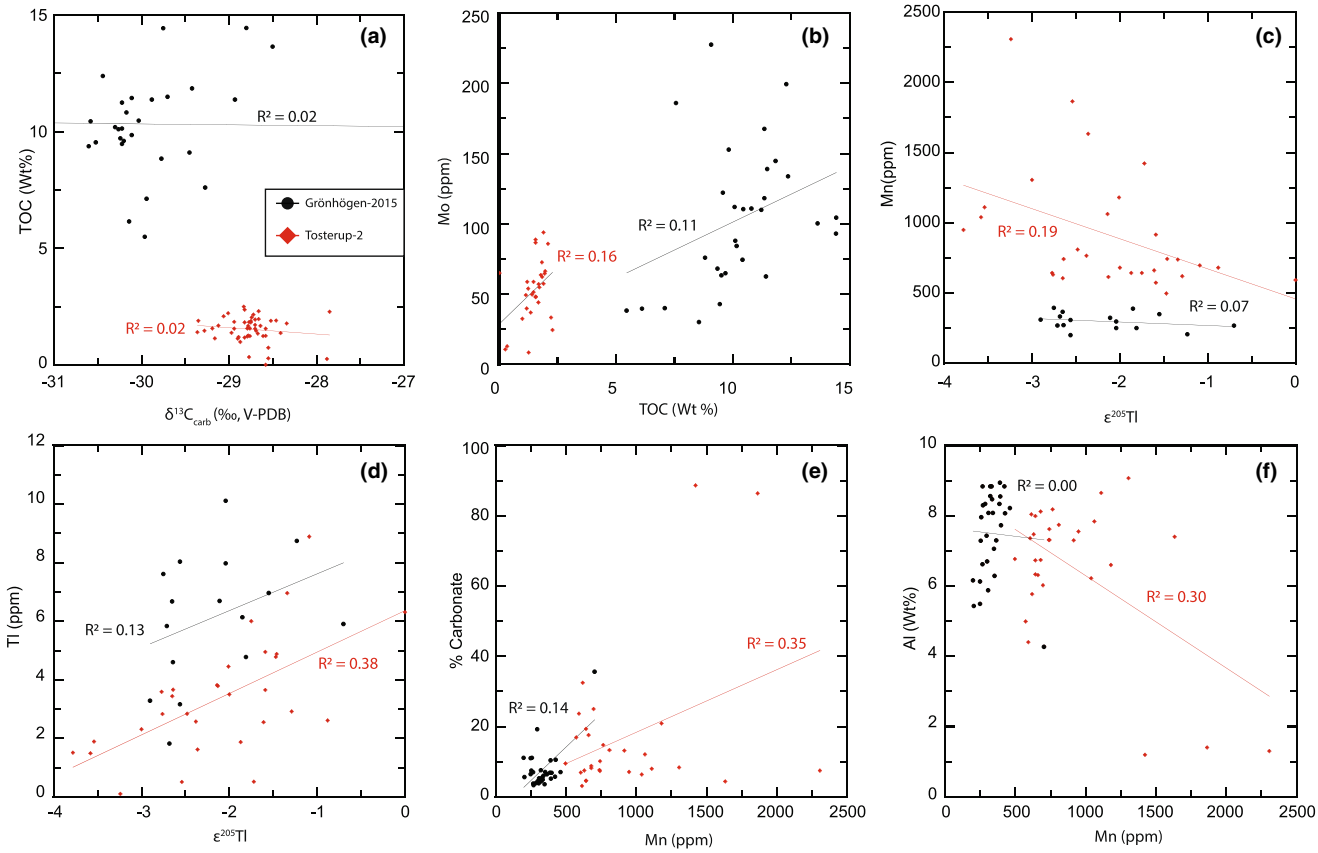

FIGURE 4 Cross-plots of geochemical data used for diagenetic alteration screening. Black circles indicate geochemical data from the Grönhögen-2015 core, and red diamonds indicate geochemical data from the Tosterup-2 core

enrichment above the typical anoxic threshold of 850 ppm in the Tosterup-2 core (Figure 4c). However, iron speciation supports that the strata of the Tosterup-2 core were locally deposited under anoxic conditions. Importantly, the negative correlation between Mn concentrations and Tl isotopic compositions is antithetical to expected trends if $\varepsilon^{205}Tl_{auth}$ were primarily controlled by local burial of Mn-oxides. This suggests that Tl isotopic compositions reflect seawater values rather than local Mn-oxide influenced values despite higher Mn concentrations. Potential sources of Mn may be lithogenically derived (i.e., terrigenous input) or sourced from Mn-carbonates (i.e., the 'orsten' beds or stinkstones; see further explanations in Section 5.1).

In this study, we will interpret both local and global changes in marine paleoredox across the late Cambrian–Early Ordovician transition. Iron speciation provides independent local water column constraints and indicate persistent anoxic conditions throughout the studied intervals of both drill cores. In conjunction with Mn concentrations, this eliminates fluctuations in local redox conditions as primary controls on trace metal enrichments that are recorded in both of our drill core successions. Thus, we utilize our trace metal datasets presented here for global marine redox interpretations, specifically with regards to Mo and V marine reservoir sizes. Our Tl isotopic trends provide insights into global fluctuations of Mn-oxide burial which is directly related to mildly reducing conditions throughout the late Cambrian–Early Ordovician. These combined local and global perspectives will then be placed into the context of fluctuations of marine oxygen throughout the successive stages of Ordovician biodiversification.

5.1 | Local redox conditions in the Baltic Basin

The mostly depleted Mn concentrations and Mn_{EF} for both cores indicate pervasive local anoxia in the Baltic Basin during the time of deposition. The values reported are generally <850 ppm, with a total core average of ~334 ppm Mn within the Grönhögen-2015 core and an average of ~912 ppm Mn within the Tosterup-2 core. The Mn enrichment factor (Mn_{EF}) within the Grönhögen-2015 core is consistently ≤1, while Mn_{EF} is slightly higher in the Tosterup-2 core with an average value of ~3. The average Mn concentration and Mn_{EF} of the Tosterup-2 core is greater than the anoxic threshold primarily within the Early Ordovician interval of the drill core. Similarly, the Mn_{EF} for the entire core is also higher than ~1; however, this is again due to several outlier values within the Early Ordovician interval. This mild enrichment of Mn may be due to significant non-oxide forms of Mn such as Mn-carbonates or an elevated sedimentation rate within this core, and thus most of this Mn is likely lithogenic in nature. The presence of Mn-carbonates

may indicate a depositional environment near the chemocline as observed in the modern-day Black Sea, commonly referred to as the "bathtub ring" in which the mixing between oxic and anoxic waters occurs (Force & Maynard, 1991). Indeed, cross-plots between Mn and carbonate content (total inorganic carbon; TIC or % Carbonate) show a weak correlation (Grönhögen-2015 $R^2 = 0.14$; Tosterup-2 $R^2 = 0.35$), suggesting some influence of Mn-carbonates on total Mn concentrations within both cores. Lastly, the slightly high sedimentation rate (averaged sedimentation rate of ~4.65 m/Myr) may be related to non-oxide Mn from a terrigenous source as there is some covariation between Al and Mn content ($R^2 = 0.30$; Figure 4f). The presence of non-oxide forms of Mn will not significantly influence Tl isotopic compositions, and thus we interpret changes in $\varepsilon^{205}Tl_{auth}$ to reflect secular changes in seawater compositions, and ultimately changes in global Mn-oxide burial in the latest Cambrian through earliest Ordovician.

Throughout the analyzed study intervals, our iron geochemistry indicates persistently reducing bottom water conditions for the Baltic Basin. Both the Grönhögen-2015 and Tosterup-2 cores show Fe_{HR}/Fe_T values above the possibly anoxic threshold of 0.22, as well as values that plot mostly above the anoxic threshold of 0.38 (Raiswell et al., 2018). Iron speciation also confirms that the Baltic Basin experienced euxinic conditions as Fe_{pyr}/Fe_{HR} data are all consistently above the threshold values for euxinia (values above 0.78) in both cores, apart from a few meters within the lower portion of the Tosterup-2 core. Latest Cambrian through earliest Ordovician strata within the Grönhögen-2015 core contain values of Fe_{HR}/Fe_T near or slightly below the 0.38 threshold, and could possibly indicate deposition within less reducing conditions, but this interval coincides with highly enriched Mo concentrations (see further discussion of Mo below). This interval generally contains [Mo] >100 ppm and/or [V] ≈ 1000 ppm, which requires persistent water-column euxinia, with anoxia as a prerequisite (Algeo & Rowe, 2012; Scott & Lyons, 2012; Tribovillard et al., 2006). Alternatively, this sudden shift in iron speciation toward values between 0.22 and 0.38 (within the upper *C. tumida* trilobite Biozone) may be the result of a strengthening iron shuttle, moving highly reactive iron to deeper portions of the basin, similar to that found in modern Black Sea (Severmann et al., 2010). Near permanent euxinic conditions as indicated by Fe speciation are also supported by the overall high concentrations of Mo >100 ppm throughout most of the two cores, with the exception of a few intervals where concentrations of Mo fall between 30 and 100 (see further trace metal discussion below). Generally, enrichments >100 ppm are difficult to obtain without persistent sulfidic water column conditions (Scott & Lyons, 2012). The very high enrichment factors calculated for both V and Mo for both drill core datasets (i.e., V_{EF} and Mo_{EF} » 10) indicate open marine to possibly semi-restricted basin conditions (Algeo & Tribovillard, 2009). As a result of these high enrichment factors in both drill core successions, the trends in [V, Mo] are more likely to reflect changes in marine trace metal inventories than changes basin connectivity throughout the late Cambrian–Early Ordovician.

5.2 | Late Cambrian–early Ordovician global ocean redox conditions

The local paleoredox conditions are constrained by both the low Mn concentrations and iron speciation, which strongly indicate that bottom waters within this portion of the Baltic Basin were persistently anoxic and euxinic. With these independent constraints on local paleoredox established, the broader-scale patterns of trace metal concentrations (e.g., Mo, V) are likely to be reflective of changes in global marine inventories rather than local cycling of V and Mo. In both cores, noticeable shifts in Cambrian and Ordovician average concentrations of V and Mo are interpreted to reflect changes in global seafloor extent of anoxia and euxinia. Concentrations of V in the late Cambrian are significantly enriched above upper continental crust values (UCC; ~60 ppm; Taylor & McLennan, 1995), and range between ~150 and 3500 ppm with an average of ~900 ppm. However, this late Cambrian average [V] is lower than the Ordovician average value of ~1600 ppm, with a range between ~180 and 3500 ppm in the Ordovician portions of these drill cores. These smaller enrichments of V found in the Baltic Basin throughout the Paibian–Stage 10 strata are best interpreted as being due to extensive drawdown of late Cambrian V marine inventories, potentially driven by expansive oxygen minimum zones (OMZs) on continental margins (Algeo, 2004; Reinhard et al., 2013). Similar mechanisms have been proposed for Cretaceous Oceanic Anoxic Event 2 (OAE2), the late Devonian mass extinction and potentially for early Silurian CIEs where relatively extensive sea floor anoxia and euxinia have been shown to impact global trace metal reservoirs (Algeo, 2004; Goldberg et al., 2016; Hetzel et al., 2009; Young et al., 2020). Corresponding concentrations of Mo from late Cambrian strata (~12–230 ppm, average ~ 95 ppm) are significantly enriched compared to Early Ordovician values (~12–230 ppm, average ~ 60 ppm). These large enrichments of Mo within late Cambrian reflect a relatively large marine Mo inventory, and thus indicates that there was a limited global extent of euxinia within the overall more expansive late Cambrian OMZs (Figure 5a).

The Early Ordovician (Tremadocian) trace metal datasets show opposite trends in [V] and [Mo] when compared to the underlying late Cambrian strata trace metal enrichment patterns. There are larger V enrichments and lowered Mo enrichments in our Ordovician intervals of both cores; average V is ~1600 ppm and average Mo ~60 ppm for the Ordovician strata vs. average V ~ 900 ppm and average Mo ~95 ppm for the late Cambrian strata. We attribute these trends to an overall reduction in global anoxic seafloor extent, which would have allowed for an increase in the overall V marine inventory. Meanwhile, the lowered enrichments of [Mo] likely reflect an expansion of euxinic bottom waters within the remaining Early Ordovician OMZs (Figure 5b). This expansion of euxinic extent allows for extensive Mo drawdown of Early Ordovician marine inventories within persistently euxinic basins, such as the Baltic Basin, as these conditions are highly efficient in sequestering Mo, thus limiting the ability for larger local enrichments (Algeo, 2004; Reinhard et al., 2013).

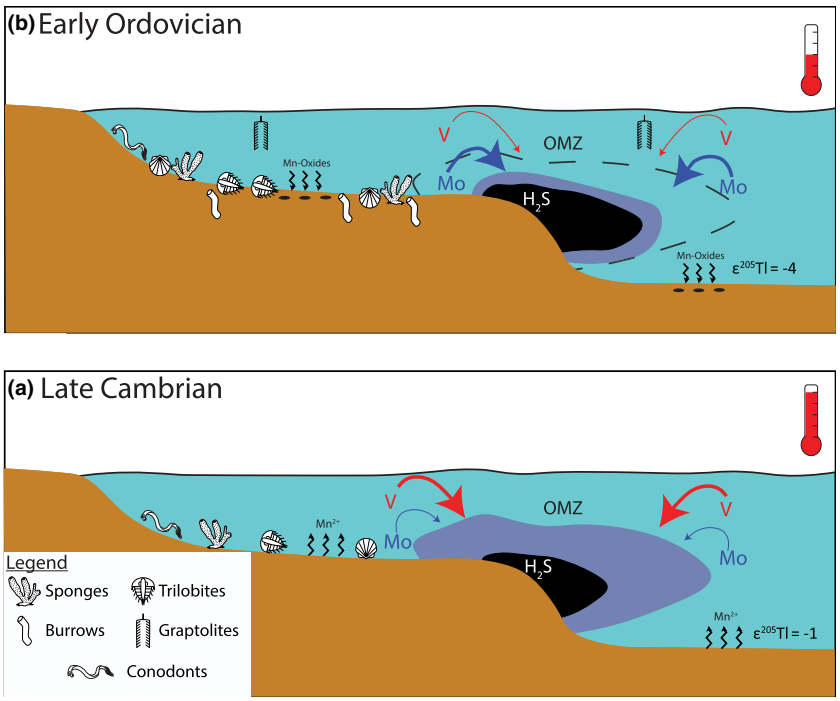

FIGURE 5 Reconstruction of typical late Cambrian and Early Ordovician margins. Changes in anoxic (purple) and euxinic (black) extent are based on V and Mo dynamics as discussed in the text. Changes in Mn-oxide formation and burial are based on Tl isotopic changes. The late Cambrian is characterized by largely reducing conditions, and an overall reduced capacity for form and bury Mn-oxides when compared to the Early Ordovician. The release of aqueous Mn^{2+} would occur wherever condition do not allow for the long-term burial of Mn-oxides. The relative abundance of fauna indicates relative changes in biodiversity of that faunal group

The local proportion of (non-sulfidic) anoxic and sulfidic/euxinic conditions within OMZs are thought to be controlled by several local factors including: intensity of primary productivity, ocean circulation patterns, changes in dissolved O_2 conditions, ambient atmospheric O_2 concentrations, and the localized availability of terminal electron acceptors of anerobic respiration prior to sulfate reduction (i.e., availability of Mn, NO_3^-, and Fe; Ulloa et al., 2012; Callbeck et al., 2021 and references therein). Increases in primary productivity would increase total remineralization rates, increasing both aerobic and anerobic respiration rates, ultimately providing a mechanism to increase the total extent of strongly reducing conditions (i.e., sulfidic/euxinia). Meanwhile, an increase in available Mn, NO_3^-, and Fe would ultimately reduce the extent of sulfidic/euxinic conditions while increasing the extent of non-sulfidic anoxia, as enhanced anaerobic respiration prior to sulfate reduction would ultimately decrease the total available organic matter for sulfate reduction. Lastly, changes in local circulation patterns and/or local ventilation would provide additional O_2 available for aerobic respiration, ultimately reducing availability of organic matter utilized in subsequent anaerobic respiration. Fluctuations in global productivity, global availability in Mn, NO_3^-, and Fe, and/or changes in global circulation patterns may ultimately provide potential mechanism(s) for the fluctuations in marine inventories of these redox-sensitive metals. However, this multiproxy dataset surrounding the late Cambrian–Early Ordovician interval is unable to ascertain which of these primary causal mechanism(s) may have been responsible for these fluctuations in marine geochemical records. Further studies are required to unambiguously reconstruct changes in local to global primary productivity, global cycling of Mn, NO_3^-, and Fe and/or, ocean circulation dynamics across this interval.

Lastly, our new Tl isotopic records show peak values of $\varepsilon^{205}Tl_{auth} \approx -1$ in the uppermost Cambrian, which trend toward lighter values in the Lower Ordovician (to $\varepsilon^{205}Tl_{auth} \approx -4$), likely corresponding to protracted changes in the burial flux of Mn-oxides. Specifically, throughout the Paibian to lowermost Stage 10, Tl isotopes increase from $\varepsilon^{205}Tl_{auth} \approx -2.5$ to -1, which likely represents a modest overall reduction in the global burial of Mn-oxides, and thus a possible expansion of anoxic conditions. These values largely fall within the accepted range of bulk crustal values ($\varepsilon^{205}Tl_{bulk} = -2 \pm 1.0$), potentially indicating a near absence of Mn-oxide burial throughout this interval of time in the late Cambrian–earliest Ordovician. An additional interpretation for these heavy Tl isotopic values, that appear nearly indistinguishable from bulk crustal values, may represent a highly restricted basin similar to that of the Black Sea, where $\varepsilon^{205}Tl_{seawater} = \sim -2$. The Black Sea, being a highly reducing basin effectively buries no Mn-oxides, and largely records Tl isotopic compositions similar to input values (Owens et al., 2017). The Baltic Basin is not thought to be highly restricted, as seen by the geographically widespread trilobite faunas and protoconodonts found within the late Cambrian portions of the cores and nearby outcrops, and the globally recognized graptolite faunas found in the Early Ordovician intervals (Ahlberg et al., 2019; Terfelt et al., 2014). Furthermore, the extreme enrichments of redox-sensitive metals such as V and Mo, which require a large open marine reservoir (Scott & Lyons, 2012), indicate little to no basin restriction during the studied interval. Lastly, the preservation of secular seawater Tl isotopic compositions is further supported through cross-plots of the leached fraction of Tl presumably adsorbed to pyrite, compared to Al derived from lithogenic sources (Nielsen et al., 2011). We identify variable, but generally better correlation between pyrite content and leached Tl in our samples, when compared to the poor correlation between total Al and leached Tl (Figure 4g,h). The poor and possibly negative correlation between the leached Tl fraction and Al suggests that detrital delivery of Tl is unlikely to be a major controlling mechanism for the observed $\varepsilon^{205}Tl_{auth}$

trends recorded in our studied drill cores. Meanwhile, authigenic Tl is thought to be adsorbed to pyrite in sulfidic environments, which is supported by the correlations between the leached Tl fraction and pyrite (Nielsen et al., 2011; Owens et al., 2017). Ultimately, this suggests that our presented authigenic Tl isotopic trends reflect authigenic Tl rather than lithogenic derived overprinting of bulk crustal Tl isotope values. Thus, given the multiple lines of evidence discussed here, we largely interpret these more positive Tl isotope values as indicating widespread anoxia. This was apparently the predominant global paleoredox backdrop throughout the Jiangshanian, in which the extent of highly reducing conditions, that is, euxinic conditions, were fluctuating within and linked to the biomere extinction during this interval of the late Cambrian (base Sunwaptan extinctions; Taylor et al., 2012; Adrain et al., 2014; Saltzman et al., 2015). These reducing conditions continued to expand, as indicated by the heaviest values of $\varepsilon^{205}Tl_{auth} \approx -1$, until the beginning of the TOCE interval (middle Stage 10 if defined by the First Appearance Datum of *Lotagnostus americanus*), where Tl isotope values begin to decrease (Figure 2). This change in $\varepsilon^{205}Tl_{auth}$ during the middle–late Stage 10 suggests a potential waning of reducing conditions in the global oceans, and is broadly coincident with the base Skullrockian biomere extinction (Adrain et al., 2014; Taylor et al., 2012). This decrease in extent of marine reducing conditions is indicated by the protracted decline in Tl isotope values from $\varepsilon^{205}Tl_{auth} \approx -1$ to −4 that spans late Stage 10 through the early Tremadocian interval (Figure 3). This decreasing trend in Tl isotopes broadly supports our interpretations of the corresponding trace metal enrichment trends from the late Cambrian into the Early Ordovician, specifically [V], as this element primarily responds to anoxia rather than euxinia (Tribovillard et al., 2006). The interpretations regarding the decreases in Tl isotopic composition are consistent with a decrease in overall reducing conditions, similar to other studies (Fan et al., 2020; Newby et al., 2021; Ostrander et al., 2019, 2020). Here we interpret this decreasing trend as a reduction of bottom water extent of OMZs from late Cambrian into the Early Ordovician oceans. This allowed for more seafloor environments to become favorable areas for oxidation and burial of additional Mn.

5.3 | Oceanographic changes and its influences on early Paleozoic biodiversity

Trends within this new dataset of trace metal contents and Tl isotopic compositions shed new light on a longer-term fluctuation in the paleoredox landscape from the latest Cambrian through Early Ordovician. Changing redox conditions have been proposed as a mechanism influencing changes in biodiversity. An expansion of reducing conditions has previously been proposed to explain the base Steptoean and base Sunwaptan biomere extinctions that surround the SPICE interval through the sulfur isotopic compositions of carbonate-associated sulfate and sedimentary pyrite ($\delta^{34}S_{CAS}$ and $\delta^{34}S_{pyr}$, respectively), iron speciation, and seawater Mo inventory drawdown (Gill et al., 2011; LeRoy & Gill, 2019). We find broad support for this previous hypothesis for expansion of highly reducing conditions surrounding the base Sunwaptan extinction from our geochemical datasets presented here, as seen in the drawdown of V and heavy $\varepsilon^{205}Tl_{auth}$ values within the falling limb interval of the SPICE (Figure 2). While [V] and Tl isotopes do not directly track euxinic conditions, they do suggest that non-sulfidic reducing conditions were pervasive during the Jiangshanian Age, which is a prerequisite for euxinia and again consistent with global expansion marine reducing conditions during this time (Gill et al., 2011).

To our knowledge, no dataset has focused on linking changes in global and/or local marine reducing conditions to the base Skullrockian biomere extinction. We estimate that the base of the *A. ecorne* trilobite Biozone occurs at ~ −4.0 m in the Tosterup-2 drill core, which is approximately equivalent to the base of the *Cordylodus proavus* conodont Biozone, in turn coincident with the base of the Skullrockian Stage in North America and the associated biomere extinction event (for trilobite and conodont biostratigraphic schemes, see Taylor et al., 2012 and Terfelt et al., 2014). Previous biostratigraphic and carbon isotope studies have identified the TOCE/HERB in both of our studied drill cores (Ahlberg et al., 2019; Terfelt et al., 2014), and this perturbation of the global carbon cycle occurs just prior to the base Skullrockian biomere extinction interval (Figure 3). Interestingly, our new data suggest a noticeable shift toward lighter $\varepsilon^{205}Tl_{auth}$ values (from ~ −1 to ~ −3) and an increase in V concentrations (from ~500 to ~1000 ppm) that are approximately coeval with the base Skullrockian biomere extinction (Figure 3). These changes in our geochemical records may indicate a global decrease in marine reducing conditions, as latest Cambrian oceans potentially increased their capacity to bury additional Mn-oxides, as well as increased the marine inventory of vanadium. While a contraction in reducing conditions may seem counter intuitive with respect to stressors of marine biota, brief oxygenation events associated with other major mass extinctions have been documented in $\varepsilon^{205}Tl_{auth}$ records(i.e., Kozik et al., 2022; Newby et al., 2021). Brief oxygenation events like the one identified here, and in the latest Ordovician and end Permian, may have provided an additional stressor to faunas adapted to low oxygen conditions. At present, the data presented herein represent the only known paleoredox records spanning the base Skullrockian biomere extinction interval. Further paleoredox work is necessary to test our hypothesized scenario and determine the causal mechanisms for the observed geochemical trends during this interval of the latest Cambrian, and what the linkages may be for paleoredox conditions and the extinction event.

Studies have identified an expansion of reducing conditions associated with the younger base Stairsian biomere extinction through the use of iodine-to-calcium ratios (I/Ca) and $\delta^{34}S_{CAS}$ isotopic trends (Edwards et al., 2018; Saltzman et al., 2015). In these studies, extremely low I/Ca values have been interpreted to represent local water column anoxia, while positive excursions of $\delta^{34}S_{CAS}$ have been interpreted as an increase in global pyrite burial within expanded euxinic settings in the global oceans. The Early Ordovician (Tremadocian) geochemical trends provide further evidence for an expansion of reducing marine conditions as a causal factor for some

biomere extinction events, as they are similar to those proposed for the older late Cambrian SPICE and associated base Steptoean and base Sunwaptan biomere extinctions (Figure 6). These datasets, in conjunction with our new trace metal and Tl isotopic profiles of older strata, provide further supporting evidence for a more variable paleoredox landscape during the late Cambrian–Early Ordovician.

Currently, the only study to reconstruct paleoredox conditions across the Cambrian–Ordovician boundary originates from the GSSP locality of the Cambrian–Ordovician boundary at Green Point, Newfoundland in Canada (Azmy et al., 2015), which utilized paired nitrogen and uranium isotopic compositions ($\delta^{15}N$ and $\delta^{238}U$, respectively). This study identified a relatively abrupt global shift to more reducing conditions prior to the Cambrian–Ordovician boundary based on $\delta^{238}U$ trends, which may potentially be captured in the Tl isotopic datasets presented here from the Tosterup-2 drill core. Unfortunately, the timing and duration inferred from the differing paleoredox studies are difficult to correlate in detail due to differences in biostratigraphic schemes (i.e., conodonts vs. trilobites) which are ultimately facies dependent and/or geographically limited. Furthermore, the degree of change in marine reducing conditions is difficult to precisely reconcile due to differences in residence times (~18 kyr for Tl vs ~450 kyr for U) of the two global paleoredox proxies used, as well as difference in proxy redox responses, with different spatiotemporal constrains (Lau et al., 2019).

The primary causal mechanisms controlling the changes in marine oxygenation surrounding the Cambrian–Ordovician boundary are poorly constrained. Changes in climate and the environment, particularly major storms and periods of high storm frequency within the latest Cambrian, have been proposed as a controlling mechanism for at least local redox conditions for the Alum Shale Formation, against the backdrop of persistent euxinia within the Baltic Basin at this time (Dahl et al., 2019). However, these local changes in paleoredox conditions would only influence the surrounding area and cannot explain the global shift to less reducing conditions as seen in the datasets presented here. Unfortunately, the global underpinning mechanisms for these fluctuations of reducing conditions surrounding this interval remains elusive and more multiproxy datasets from hydrographically dispersed basins are needed.

Our new high-resolution trace metal and Tl isotopic trends shed light on a protracted increase in bottom water oxygenation, and nuanced changes of anoxic/euxinic conditions within OMZs which may have set the stage for subsequent changes in marine biodiversity during the Ordovician (Figure 6). An overall reduction in anoxic conditions along continental margins likely contributed to the changes in ecosystem dynamics of the various steps and phases of the GOBE by expanding habitable shelf space and facilitating increased metabolic processes through increased oxygen availability (Stigall et al., 2019). Enhanced bottom water oxygen levels and potentially deeper oxygen penetration into sediments may have facilitated the increased bioturbation depth and burrowing complexity surrounding the Cambrian–Ordovician boundary (Droser & Bottjer, 1989). This notion is further supported by the abrupt increases in deep-marine ichnodiversity and ichnodisparity during the Early Ordovician (Tremadocian; Buatois et al., 2016), as greater oxygen penetration depth within marine sediments would not only facilitate new types of burrowing but also overall depth in which marine organisms could burrow. These newly oxygenated deep-marine settings would be rich in labile organic matter and

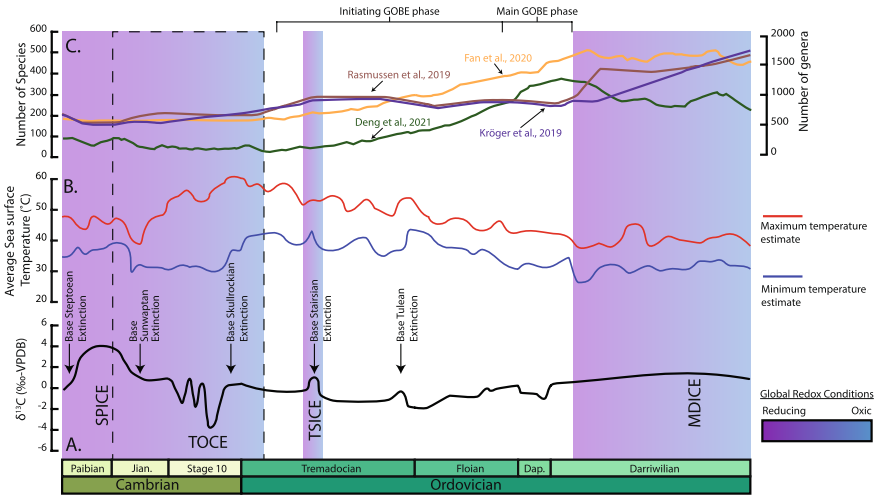

FIGURE 6 Summary of geochemical and physical palaeoceanographic trends of the late Cambrian–Early Ordovician. (a) Generalized $\delta^{13}C_{carb}$ trends of the late Cambrian–Middle Ordovician. (b) Generalized average sea surface temperature ranges for the late Cambrian–Middle Ordovician. Upper red line represents the maximum temperature estimates while the lower blue line represents minimum temperature estimates (modified from Goldberg et al., 2021). (c) Generalized biodiversity trends of the late Cambrian–Middle Ordovician, modified from Deng et al. (2021). Species axis refers to biodiversity trends of Deng et al. (2021) and Fan et al. (2020) (green and orange lines, respectively), while genera axis refers to trends from Rasmussen et al. (2019) and Kröger et al. (2019) (brown and purple lines, respectively). Gradients from purple to blue represent changes from globally reducing conditions (purple) to more oxygenated global conditions (blue). Dashed box surrounding the late Cambrian–Early Ordovician represent our study interval

thus provide important new sources of food for the burgeoning marine ecosystems of the Ordovician. In addition to increased bioturbation depth and complexity, tiering increased across the Cambrian–Ordovician boundary (Ausich & Bottjer, 1982; Bottjer & Ausich, 1986). This likely indicates enhanced water-column oxygenation. Lastly, macrofauna also increased in diversity throughout this interval on several paleocontinents, potentially showing that water column oxygenation facilitated enhanced cellular respiration needed for predation (Deng et al., 2021; Rasmussen et al., 2019). This overall reduction in areal extent of reducing conditions, via the movement of OMZs off continental shelves and/or an overall reduction of OMZ extent, would likely increase the overall habitable ecospace, fueling the subsequent Ordovician rise in biodiversity.

A progressive increase in marine oxygen levels has been postulated as one of many factors that facilitated the overall increase in biodiversity leading into the main phase of the GOBE (Dapingian–early Darriwilian). A lack of direct paleoredox studies throughout the late Cambrian to Middle Ordovician has led to coarse resolution in atmospheric and marine oxygen models, and thus these models commonly disagree in terms of oxygenation trends through this interval (Edwards et al., 2017; Krause et al., 2018; Lenton et al., 2018); however, all recent atmospheric oxygen models generally show an increasing trend within the Late Ordovician. Across the Cambrian–Ordovician boundary most models generally show low pO_2, ranging between 2% and 10% (Dahl et al., 2010; Krause et al., 2018; Lenton et al., 2018; Sperling et al., 2015). Our dataset currently agrees most with the GEOCARBSULFOR model proposed by Krause et al. (2018), which shows a large increase in pO_2 surrounding the Cambrian–Ordovician boundary, broadly consistent with the long-term trend toward more negative Tl isotope values and increases in V concentrations. Unfortunately, there are very few studies throughout most of the Early and Middle Ordovician (Tremadocian–Dapingian) that utilize direct marine paleoredox proxies, with the exception of the base Stairsian biomere extinction interval (Figure 6). Therefore, future detailed paleoredox investigations are needed to gain better insights into the role of oxygen in the early phases of the GOBE.

6 | CONCLUSIONS

Our new iron speciation, trace element, and Tl isotopic records have revealed nuanced and significant changes in global paleoredox conditions during the late Cambrian–Early Ordovician interval. Iron speciation datasets indicate that local bottom water conditions were persistently anoxic and/or euxinic within the Baltic Basin. The trends and variations in V and Mo concentrations indicate that global marine trace metal inventories fluctuated significantly due to the total seafloor extent of anoxia and euxinia, respectively. Here we conclude that widespread anoxia in the form of large-scale OMZs, with limited euxinic fractions within them, likely dominated late Cambrian marine redox landscapes. In contrast, the Early Ordovician appears to have seen an overall reduction in anoxic seafloor extent, but within the remaining OMZs euxinic conditions likely expanded. This overall reduction in OMZ extent, inferred from changes in enrichment patterns in V and Mo concentrations, is corroborated by our novel Tl isotopic dataset. The collective data suggest that there was an enhanced capacity for the formation and burial of Mn-oxides in the oceans in the time leading into and during the Early Ordovician.

This dynamic paleoredox landscape may be intimately linked to variations in biodiversity, as documented throughout the late Cambrian–Early Ordovician. The widespread anoxic conditions throughout the late Cambrian–Early Ordovician may be responsible for the frequency of the biomere extinctions as well as the apparently elevated background extinction rate (e.g., Steptoean, Sunwaptan and Stairsian biomere extinctions). Meanwhile, fewer biomere extinctions and lowered extinction rates may be linked to the contraction of these reducing conditions in the Early Ordovician. In addition, this global contraction of reducing conditions in the Early Ordovician may have prompted an increase in ichnofacies, tiering and macrofaunal diversity in the Early Ordovician during the initiation of the GOBE. Ultimately, enhanced oxygen penetration into sediments and water columns led to expanded niche space due to newly oxygenated shelf areas and thus facilitated the GOBE.

ACKNOWLEDGMENTS

We thank three anonymous reviewers for their detailed and constructive comments that helped to significantly improve earlier versions of this manuscript, as well as Nicholas Butterfield for editorial guidance. We would like to thank Sean Newby, Lindsi Allman, and Jane Wadhams for their assistance with geochemical analysis, Frans Lundberg, Mikael Erlström and the Geological Survey of Sweden for granting access, as well as assistance in sampling the Grönhögen-2015 drill core and Jörg Maletz in assisting with the identification of graptolite faunas. This work was performed at the National High Magnetic Field Laboratory in Tallahassee, Florida, which is supported by National Science Foundation Cooperative Agreement No. DMR-1644779 and by the State of Florida. This work was supported by the National Science Foundation Cooperative Agreement No. DMR-1157490 and the State of Florida. This research was funded by the American Chemical Society Petroleum Research Fund (ACS-PRF# 57487-DNI2 to S.A.Y.), Gyllenstierna Krapperup's Foundation (grant award KR2019-0089 to P. A. and S.A.Y.), the Biirgit and Hellmuth Hertz Foundation (to A. L.), the NASA Exobiology Program (80NSSC23K0346 to S.A.Y. and J.D.O.), the Sloan Research Foundation (FG-2020–13552 to J.D.O), and the Winchester Fund (to N.P.K.).

DATA AVAILABILITY STATEMENT

Data is not yet available for public use. Data tables for all geochemistry data will be made available in the data repository/supplemental information of this manuscript upon the editor's final decision of the manuscript.

ORCID

Nevin P. Kozik https://orcid.org/0000-0001-7759-7552

REFERENCES

Achab, A., & Paris, F. (2007). The Ordovician chitinozoan biodiversification and its leading factors. *Palaeogeography, Palaeoclimatology, Palaeoecology*, *245*, 5–19.

Adrain, J. M., Westrop, S. R., Karim, T. S., & Landing, E. D. (2014). Trilobite biostratigraphy of the Stairsian stage (upper Tremadocian) of the Ibexian series, lower Ordovician, western United States. *Memoirs of the Association of Australasian Palaeontologists*, *1*, 167–214.

Ahlberg, P. E. R., Lundberg, F., Erlström, M., Calner, M., Lindskog, A., Dahlqvist, P., & Joachimski, M. M. (2019). Integrated Cambrian biostratigraphy and carbon isotope chemostratigraphy of the Grönhögen-2015 drill core, Öland, Sweden. *Geological Magazine*, *156*, 935–949.

Algeo, T. J. (2004). Can marine anoxic events draw down the trace element inventory of seawater? *Geology*, *32*, 1057–1060.

Algeo, T. J., & Lyons, T. W. (2006). Mo-total organic carbon covariation in modern anoxic marine environments: Implications for analysis of paleoredox and paleohydrographic conditions. *Paleoceanography*, *21*, 1–23.

Algeo, T. J., & Maynard, J. B. (2008). Trace-metal covariation as a guide to water-mass conditions in ancient anoxic marine environments. *Geosphere*, *4*, 872–887.

Algeo, T. J., & Rowe, H. (2012). Paleoceanographic applications of trace-metal concentration data. *Chemical Geology*, *324–325*, 6–18.

Algeo, T. J., & Tribovillard, N. (2009). Environmental analysis of paleoceanographic systems based on molybdenum-uranium covariation. *Chemical Geology*, *268*, 211–225.

Anbar, A. D., Duan, Y., Lyons, T. W., Arnold, G. L., Kendall, B., Creaser, R. A., Kaufman, A. J., Gordon, G. W., Scott, C., Garvin, J., & Buick, R. (2007). A whiff of oxygen before the great oxidation event? *Science*, *317*, 1903–1906.

Ausich, W. I., & Bottjer, D. J. (1982). Tiering in suspension-feeding communities on soft substrata throughout the Phanerozoic. *Science*, *216*, 173–174.

Azmy, K., Kendall, B., Brand, U., Stouge, S., & Gordon, G. W. (2015). Redox conditions across the Cambrian-Ordovician boundary: Elemental and isotopic signatures retained in the GSSP carbonates. *Palaeogeography, Palaeoclimatology, Palaeoecology*, *440*, 440–454.

Bottjer, D. J., & Ausich, W. I. (1986). Phanerozoic development of Tiering in soft substrata suspension-feeding communities. *Paleobiology*, *12*, 400–420.

Bowman, C. N., Young, S. A., Kaljo, D., Eriksson, M. E., Them, T. R., Hints, O., Martma, T., & Owens, J. D. (2019). Linking the progressive expansion of reducing conditions to a stepwise mass extinction event in the late Silurian oceans. *Geology*, *47*, 968–972.

Brüchert, V., & Pratt, L. M. (1996). Contemporaneous early diagenetic formation of organic and inorganic sulfur in estuarine sediments from St. Andrew bay, Florida, USA. *Geochimica et Cosmochimica Acta*, *60*, 2325–2332.

Buatois, L. A., Mángano, M. G., Olea, R. A., & Wilson, M. A. (2016). Decoupled evolution of soft and hard substrate communities during the Cambrian explosion and great ordovician biodiversification event. *Proceedings of the National Academy of Sciences of the United States of America*, *113*, 6945–6948.

Callbeck, C. M., Canfield, D. E., Kuypers, M. M. M., Yilmaz, P., Lavik, G., Thamdrup, B., Schubert, C. J., & Bristow, L. A. (2021). Sulfur cycling in oceanic oxygen minimum zones. *Limnology and Oceanography*, *66*, 2360–2392.

Calvert, S. E., & Pedersen, T. F. (1996). Sedimentary geochemistry of manganese: Impliations for the Enviroment of formation of Manganiferous black shales. *Economic Geology*, *91*, 36–47.

Cocks, L. R. M., & Torsvik, T. H. (2005). Baltica from the late Precambrian to mid-Palaeozoic times: The gain and loss of a terrane's identity. *Earth-Science Reviews*, *72*, 39–66.

Dahl, T. W., Hammarlund, E. U., Anbar, A. D., Bond, D. P. G., Gill, B. C., Gordon, G. W., Knoll, A. H., Nielsen, A. T., Schovsbo, N. H., & Canfield, D. E. (2010). Devonian rise in atmospheric oxygen correlated to the radiations of terrestrial plants and large predatory fish. *Proceedings of the National Academy of Sciences of the United States of America*, *107*, 17911–17915.

Dahl, T. W., Siggaard-Andersen, M. L., Schovsbo, N. H., Persson, D. O., Husted, S., Hougård, I. W., Dickson, A. J., Kjær, K., & Nielsen, A. T. (2019). Brief oxygenation events in locally anoxic oceans during the Cambrian solves the animal breathing paradox. *Scientific Reports*, *9*, 1–9.

Deng, Y., Fan, J., Zhang, S., Fang, X., Chen, Z., Shi, Y., Wang, H., Wang, X., Yang, J., Hou, X., Wang, Y., Zhang, Y., Chen, Q., Yang, A., Fan, R., Dong, S., Xu, H., & Shen, S. (2021). Timing and patterns of the great Ordovician biodiversification event and late Ordovician mass extinction: Perspectives from South China. *Earth-Science Reviews*, *220*, 103743.

Droser, M. L., & Bottjer, D. J. (1989). Ordovician increase in extent and depth of bioturbation: Implications for understanding early Paleozoic ecospace utilization. *Geology*, *17*, 850–852.

Droser, M. L., & Bottjer, D. J. (1993). Trends and patterns of Phanerozoic ichnofabrics. *Annual Review of Earth and Planetary Sciences*, *21*, 205–225.

Edwards, C. T., Fike, D. A., Saltzman, M. R., Lu, W., & Lu, Z. (2018). Evidence for local and global redox conditions at an early Ordovician (Tremadocian) mass extinction. *Earth and Planetary Science Letters*, *481*, 125–135.

Edwards, C. T., Saltzman, M. R., Royer, D. L., & Fike, D. A. (2017). Oxygenation as a driver of the great Ordovician biodiversification event. *Nature Geoscience*, *10*, 925–929.

Erickson, B. E., & Helz, G. R. (2000). Molybdenum (VI) speciation in sulfidic waters: Stability and lability of thiomolybdates. *Geochimica et Cosmochimica Acta*, *64*, 1149–1158.

Fan, H., Nielsen, S. G., Owens, J. D., Auro, M., Shu, Y., Hardisty, D. S., Horner, T. J., Bowman, C. N., Young, S. A., & Wen, H. (2020). Constraining oceanic oxygenation during the Shuram excursion in South China using thallium isotopes. *Geobiology*, *18*, 348–365.

Force, E. R., & Maynard, J. B. (1991). Manganese: Syngenetic deposits on the margins of anoxic basins. *Reviews on Economic Geology*, *5*, 147–157.

Froelich, P. N., Klinkhammer, G. P., Bender, M. L., Luedtke, N. A., Heath, G. R., Cullen, D., Dauphin, P., Hammond, D., Hartman, B., & Maynard, V. (1979). Early oxidation of organic matter in pelagic sediments of the eastern equatorial Atlantic: Suboxic diagenesis. *Geochimica et Cosmochimica Acta*, *43*, 1075–1090.

Gill, B. C., Lyons, T. W., Young, S. A., Kump, L. R., Knoll, A. H., & Saltzman, M. R. (2011). Geochemical evidence for widespread euxinia in the later Cambrian Ocean. *Nature*, *469*, 80–83.

Goldberg, S. L., Present, T. M., Finnegan, S., & Bergmann, K. D. (2021). A high-resolution record of early Paleozoic climate. *Proceedings of the National Academy of Sciences of the United States of America*, *118*, 1–8.

Goldberg, T., Poulton, S. W., Wagner, T., Kolonic, S. F., & Rehkämper, M. (2016). Molybdenum drawdown during cretaceous oceanic anoxic event 2. *Earth and Planetary Science Letters*, *440*, 81–91.

Hardisty, D. S., Lyons, T. W., Riedinger, N., Isson, T. T., Owens, J. D., Aller, R. C., Rye, D. M., Planavsky, N. J., Reinhard, C. T., Gill, B. C., Masterson, A. L., Asael, D., & Johnston, D. T. (2018). An evaluation of sedimentary molybdenum and iron as proxies for pore fluid paleoredox conditions. *American Journal of Science*, *318*, 527–556.

Hayes, J. M., Strauss, H., & Kaufman, A. J. (1999). The abundance of 13C in marine organic matter and isotopic fractionation in the global

biogeochemical cycle of carbon during the past 800 ma. *Chemical Geology*, *161*, 103–125.

Hetzel, A., Böttcher, M. E., Wortmann, U. G., & Brumsack, H. J. (2009). Paleo-redox conditions during OAE 2 reflected in demerara rise sediment geochemistry (ODP leg 207). *Palaeogeography, Palaeoclimatology, Palaeoecology*, *273*, 302–328.

Kozik, N. P., Young, S. A., Newby, S. M., Liu, M., Chen, D., Hammarlund, E. U., Bond, D. P. G., Them, T. R., II, & Owens, J. D. (2022). Rapid marine oxygen variability: Driver of the late Ordovician mass extinction. *Science Advances*, *8345*, 1–9.

Krause, A. J., Mills, B. J. W., Zhang, S., Planavsky, N. J., Lenton, T. M., & Poulton, S. W. (2018). Stepwise oxygenation of the Paleozoic atmosphere. *Nature Communications*, *9*, 1–10.

Kröger, B., Franeck, F., & Rasmussen, C. M. Ø. (2019). The evolutionary dynamics of the early Palaeozoic marine biodiversity accumulation. *Proceedings of the Royal Society B: Biological Sciences*, *286*, 3–8. https://doi.org/10.1098/rspb.2019.1634

Lau, K. V., Romaniello, S. J., & Zhang, F. (2019). *The uranium isotope paleoredox proxy*. Moss Landing Marine.

Lenton, T. M., Daines, S. J., & Mills, B. J. W. (2018). COPSE reloaded: An improved model of biogeochemical cycling over Phanerozoic time. *Earth-Science Reviews*, *178*, 1–28.

LeRoy, M. A., & Gill, B. C. (2019). Evidence for the development of local anoxia during the Cambrian SPICE event in eastern North America. *Geobiology*, *17*, 381–400.

Maletz, J., Zhu, X., & Zhang, Y. (2022). Graptolithina from the Guole Biota (Furongian, upper Cambrian) of South China. *Palaeoworld*, *31*(4), 582–590. https://doi.org/10.1016/j.palwor.2022.03.002

Meyers, P. A. (1994). Preservation of elemental and isotopic source identification of sedimentary organic matter. *Chemical Geology*, *114*, 289–302.

Newby, S. M., Owens, J. D., Schoepfer, S. D., & Algeo, T. J. (2021). Transient Ocean oxygenation at end-Permian mass extinction onset shown by thallium isotopes. *Nature Geoscience*, *14*, 678–683.

Nielsen, A. T., Høyberget, M., & Ahlberg, P. (2020). The Furongian (upper Cambrian) alum shale of Scandinavia: Revision of zonation. *Lethaia*, *53*, 462–485.

Nielsen, A. T., & Schovsbo, N. H. (2011). The lower Cambrian of Scandinavia: Depositional environment, sequence stratigraphy and palaeogeography. *Earth-Science Reviews*, *107*, 207–310.

Nielsen, S. G., Goff, M., Hesselbo, S. P., Jenkyns, H. C., LaRowe, D. E., & Lee, C. T. A. (2011). Thallium isotopes in early diagenetic pyrite – a paleoredox proxy? *Geochimica et Cosmochimica Acta*, *75*, 6690–6704.

Nielsen, S. G., Rehkämper, M., Porcelli, D., Andersson, P., Halliday, A. N., Swarzenski, P. W., Latkoczy, C., & Günther, D. (2005). Thallium isotope composition of the upper continental crust and rivers – an investigation of the continental sources of dissolved marine thallium. *Geochimica et Cosmochimica Acta*, *69*, 2007–2019.

Ostrander, C. M., Nielsen, S. G., Owens, J. D., Kendall, B., Gordon, G. W., Romaniello, S. J., & Anbar, A. D. (2019). Fully oxygenated water columns over continental shelves before the great oxidation event. *Nature Geoscience*, *12*, 186–191.

Ostrander, C. M., Owens, J. D., & Nielsen, S. G. (2017). Constraining the rate of oceanic deoxygenation leading up to a cretaceous oceanic anoxic event (OAE-2: ~94 ma). *Science Advances*, *3*, 1–6.

Ostrander, C. M., Owens, J. D., Nielsen, S. G., Lyons, T. W., Shu, Y., Chen, X., Sperling, E. A., Jiang, G., Johnston, D. T., Sahoo, S. K., & Anbar, A. D. (2020). Thallium isotope ratios in shales from South China and northwestern Canada suggest widespread O_2 accumulation in marine bottom waters was an uncommon occurrence during the Ediacaran period. *Chemical Geology*, *557*, 119856.

Owens, J. D. (2020). *Application of Thallium Isotopes: Tracking Marine Oxygenation through Manganese Oxide Burial (Elements in Geochemical Tracers in Earth System Science)*. Cambridge University Press. https://doi.org/10.1017/9781108688697

Owens, J. D., Nielsen, S. G., Horner, T. J., Ostrander, C. M., & Peterson, L. C. (2017). Thallium-isotopic compositions of euxinic sediments as a proxy for global manganese-oxide burial. *Geochimica et Cosmochimica Acta*, *213*, 291–307.

Owens, J. D., Reinhard, C. T., Rohrssen, M., Love, G. D., & Lyons, T. W. (2016). Empirical links between trace metal cycling and marine microbial ecology during a large perturbation to Earth's carbon cycle. *Earth and Planetary Science Letters*, *449*, 407–417.

Palmer, A. R. (1984). The biomere problem: Evolution of an idea. *Journal of Paleontology*, *58*, 599–611.

Pasquier, V., Fike, D. A., Révillon, S., & Halevy, I. (2022). A global reassessment of the controls on iron speciation in modern sediments and sedimentary rocks: A dominant role for diagenesis. *Geochimica et Cosmochimica Acta*, *335*, 211–230.

Poulton, S. W., & Canfield, D. E. (2005). Development of a sequential extraction procedure for iron: Implications for iron partitioning in continentally derived particulates. *Chemical Geology*, *214*, 209–221.

Pulsipher, M. A., Schiffbauer, J. D., Jeffrey, M. J., Huntley, J. W., Fike, D. A., & Shelton, K. L. (2021). A meta-analysis of the Steptoean positive carbon isotope excursion: The SPICEraq database. *Earth-Science Reviews*, *212*, 103442.

Raiswell, R., Hardisty, D. S., Lyons, T. W., Canfield, D. E., Owens, J. D., Planavsky, N. J., Poulton, S. W., & Reinhard, C. T. (2018). The iron paleoredox proxies: A guide to the pitfalls, problems and proper practice. *American Journal of Science*, *318*, 491–526.

Rasmussen, C. M. Ø., Kröger, B., Nielsen, M. L., & Colmenar, J. (2019). Cascading trend of early Paleozoic marine radiations paused by late Ordovician extinctions. *Proceedings of the National Academy of Sciences of the United States of America*, *116*, 7207–7213.

Reinhard, C. T., Planavsky, N. J., Robbins, L. J., Partin, C. A., Gill, B. C., Lalonde, S. V., Bekker, A., Konhauser, K. O., & Lyons, T. W. (2013). Proterozoic Ocean redox and biogeochemical stasis. *Proceedings of the National Academy of Sciences of the United States of America*, *110*, 5357–5362.

Rue, E. L., Smith, G. J., Cutter, G. A., & Bruland, K. W. (1997). The response of trace element redox couples to suboxic conditions in the water column. *Deep-Sea Research Part I: Oceanographic Research Papers*, *44*, 113–134.

Saltzman, M. R., Edwards, C. T., Adrain, J. M., & Westrop, S. R. (2015). Persistent oceanic anoxia and elevated extinction rates separate the Cambrian and Ordovician radiations. *Geology*, *43*, 807–811.

Saltzman, M. R., Young, S. A., Kump, L. R., Gill, B. C., Lyons, T. W., & Runnegar, B. (2011). Pulse of atmospheric oxygen during the late Cambrian. *Proceedings of the National Academy of Sciences of the United States of America*, *108*, 3876–3881.

Schmitz, B., Harper, D. A. T., Peucker-Ehrenbrink, B., Stouge, S., Alwmark, C., Cronholm, A., Bergström, S. M., Tassinari, M., & Xiaofeng, W. (2008). Asteroid breakup linked to the great Ordovician biodiversification event. *Nature Geoscience*, *1*, 49–53.

Scotese, C. R. (2001). Atlas of earth history. *Aging*, *1*, 55.

Scott, C., & Lyons, T. W. (2012). Contrasting molybdenum cycling and isotopic properties in euxinic versus non-euxinic sediments and sedimentary rocks: Refining the paleoproxies. *Chemical Geology*, *324–325*, 19–27.

Servais, T., Cascales-Minana, B., & Harper, D. A. T. (2021). The great Ordovician biodiversification event (GOBE) is not a single event. *Paleontological Research*, *25*, 315–328.

Servais, T., Lehnert, O., Li, J., Mullins, G. L., Munnecke, A., Nützel, A., & Vecoli, M. (2008). The Ordovician biodiversification: Revolution in the oceanic trophic chain. *Lethaia*, *41*, 99–109.

Servais, T., Owen, A. W., Harper, D. A. T., Kröger, B., & Munnecke, A. (2010). The great Ordovician biodiversification event (GOBE): The palaeoecological dimension. *Palaeogeography, Palaeoclimatology, Palaeoecology*, *294*, 99–119.

Severmann, S., McManus, J., Berelson, W. M., & Hammond, D. E. (2010). The continental shelf benthic iron flux and its isotope composition. *Geochimica et Cosmochimica Acta*, *74*, 3984–4004.

Sperling, E. A., Wolock, C. J., Morgan, A. S., Gill, B. C., Kunzmann, M., Halverson, G. P., Macdonald, F. A., Knoll, A. H., & Johnston, D. T. (2015). Statistical analysis of iron geochemical data suggests limited late Proterozoic oxygenation. *Nature*, *523*, 451–454.

Stigall, A. L., Edwards, C. T., Freeman, R. L., & Rasmussen, C. M. Ø. (2019). Coordinated biotic and abiotic change during the great Ordovician biodiversification event: Darriwilian assembly of early Paleozoic building blocks. *Palaeogeography, Palaeoclimatology, Palaeoecology*, *530*, 249–270.

Taylor, J. F., Repetski, J. E., Loch, J. D., & Leslie, S. A. (2012). Biostratigraphy and Chronostratigraphy of the Cambrian–Ordovician great American carbonate Bank. In J. Derby, R. Fritz, S. Longacre, W. Morgan, & C. Sternbach (Eds.), *Great American carbonate Bank the geology and economic resources of the Cambrian—Ordovician Sauk Megasequence of Laurentia* (pp. 1–23). American Association of Petroleum Geologists.

Taylor, S. R., & McLennan, S. M. (1995). The geochemical the continental evolution crust. *Reviews in Mineralogy and Geochemistry*, *33*, 241–265.

Terfelt, F., Eriksson, M. E., & Schmitz, B. (2014). The Cambrian-Ordovician transition in dysoxic facies in Baltica – diverse faunas and carbon isotope anomalies. *Palaeogeography, Palaeoclimatology, Palaeoecology*, *394*, 59–73.

Them, T. R., Gill, B. C., Caruthers, A. H., Gerhardt, A. M., Gröcke, D. R., Lyons, T. W., Marroquín, S. M., Nielsen, S. G., João, P. T. A., & Owens, J. D. (2018). Thallium isotopes reveal protracted anoxia during the Toarcian (early Jurassic) associated with volcanism, carbon burial, and mass extinction. *Proceedings of the National Academy of Sciences of the United States of America*, *115*, 6596–6601.

Torsvik, T. H., Van der Voo, R., Preeden, U., Mac Niocaill, C., Steinberger, B., Doubrovine, P. V., van Hinsbergen, D. J. J., Domeier, M., Gaina, C., Tohver, E., Meert, J. G., McCausland, P. J. A., & Cocks, L. R. M. (2012). Phanerozoic polar wander, Palaeogeography and dynamics. *Earth-Science Reviews*, *114*, 325–368.

Tribovillard, N., Algeo, T. J., Lyons, T., & Riboulleau, A. (2006). Trace metals as paleoredox and paleoproductivity proxies: An update. *Chemical Geology*, *232*, 12–32.

Trotter, J. A., Williams, I. S., Barnes, C. R., Lecuyer, C., & Nicoll, R. S. (2008). Did cooling oceans trigger Ordovician biodiversification? Evidence from conodont thermometry. *Science*, *321*, 550–554.

Turgeon, S., & Brumsack, H. J. (2006). Anoxic vs dysoxic events reflected in sediment geochemistry during the Cenomanian-Turonian boundary event (cretaceous) in the Umbria-Marche Basin of Central Italy. *Chemical Geology*, *234*, 321–339.

Ulloa, O., Canfield, D. E., DeLong, E. F., Letelier, R. M., & Stewart, F. J. (2012). Microbial oceanography of anoxic oxygen minimum zones. *Proceedings of the National Academy of Sciences of the United States of America*, *109*, 15996–16003.

Wang, Y., Lu, W., Costa, K. M., & Nielsen, S. G. (2022). Beyond anoxia: Exploring sedimentary thallium isotopes in paleo-redox reconstructions from a new core top collection. *Geochimica et Cosmochimica Acta*, *333*, 347–361.

Young, S. A., Benayoun, E., Kozik, N. P., Hints, O., Martma, T., Bergström, S. M., & Owens, J. D. (2020). Marine redox variability from Baltica during extinction events in the latest Ordovician–early Silurian. *Palaeogeography, Palaeoclimatology, Palaeoecology*, *554*, 109792.

Zhao, Z., Ahlberg, P., Thibault, N., Dahl, T. W., Schovsbo, N. H., & Nielsen, A. T. (2022). High-resolution carbon isotope chemostratigraphy of the middle Cambrian to lowermost Ordovician in southern Scandinavia: Implications for global correlation. *Global and Planetary Change*, *209*, 103751.

SUPPORTING INFORMATION

Additional supporting information can be found online in the Supporting Information section at the end of this article.

How to cite this article: Kozik, N. P., Young, S. A., Lindskog, A., Ahlberg, P., & Owens, J. D. (2023). Protracted oxygenation across the Cambrian–Ordovician transition: A key initiator of the Great Ordovician Biodiversification Event? *Geobiology*, *00*, 1–16. https://doi.org/10.1111/gbi.12545